LETTERS
PUBLISHED ONLINE: 30 SEPTEMBER 2012 | DOI: 10.1038/NMAT3433
nature materials

Switching terahertz waves with gate-controlled active graphene metamaterials

Seung Hoon Lee[1†], Muhan Choi[2†], Teun-Teun Kim[1†], Seungwoo Lee[1], Ming Liu[3], Xiaobo Yin[3], Hong Kyw Choi[2], Seung S. Lee[1], Choon-Gi Choi[2], Sung-Yool Choi[4], Xiang Zhang[3,5] and Bumki Min[1*]

The extraordinary electronic properties of graphene provided the main thrusts for the rapid advance of graphene electronics[1]. In photonics, the gate-controllable electronic properties of graphene provide a route to efficiently manipulate the interaction of photons with graphene, which has recently sparked keen interest in graphene plasmonics[2–10]. However, the electro-optic tuning capability of unpatterned graphene alone is still not strong enough for practical optoelectronic applications owing to its non-resonant Drude-like behaviour. Here, we demonstrate that substantial gate-induced persistent switching and linear modulation of terahertz waves can be achieved in a two-dimensional metamaterial[11,12], into which an atomically thin, gated two-dimensional graphene layer is integrated. The gate-controllable light–matter interaction in the graphene layer can be greatly enhanced by the strong resonances of the metamaterial[13]. Although the thickness of the embedded single-layer graphene is more than six orders of magnitude smaller than the wavelength ($<\lambda/1{,}000{,}000$), the one-atom-thick layer, in conjunction with the metamaterial, can modulate both the amplitude of the transmitted wave by up to 47% and its phase by 32.2° at room temperature. More interestingly, the gate-controlled active graphene metamaterials show hysteretic behaviour in the transmission of terahertz waves, which is indicative of persistent photonic memory effects.

Terahertz frequencies are situated in the far-infrared spectra of electromagnetic radiation that inherit the richness of photonics and electronics, as well as their weaknesses[14,15]. The development of electrically tunable terahertz semiconductor devices, preferably operating at room temperature, is hindered by the limitation on the change of free carrier density, which leads to inefficient responses to terahertz radiation[16,17]. Within the past decade, considerable effort has been devoted to efficiently modulating terahertz waves, with approaches including utilization of a semiconductor two-dimensional electron gas (2DEG) system[16] and a hybridized metamaterial with a charge carrier injection/depletion scheme, such as a Schottky diode[18,19] or a high-electron-mobility transistor[20]. Among these terahertz modulators, metamaterial–semiconductor hybrid structures have shown remarkable amplitude (~30%) and phase (~32.1°) modulations whereas 2DEG systems still suffered from a limited modulation depth of ~3% at room temperature. However, these previous attempts were based on conductivity changes by charge carrier injection on bulk substrates, and the electron carrier density, especially in 2DEGs, is limited to a value of $\sim 1 \times 10^{12}$ cm^{-2} within the limit of semiconductor breakdown[4]. As a possible alternative route, graphene, a truly two-dimensional atomic system, can essentially solve these problems as it allows marked modification of the Fermi level and the corresponding charge carrier density by simple electric gating. This charge carrier handling capability in graphene is an order of magnitude larger (10^{13}–10^{14}cm^{-2}; refs 21,22) than that of conventional 2DEG systems[16,20]. Furthermore, the small effective mass of charge carriers in graphene makes it possible to fully maximize the light–matter interaction in the extreme subwavelength scale.

Defects in graphene-based devices, such as grain boundaries, adsorbed H_2O molecules and other impurities acting as charge trap sites on dielectric substrates or on a graphene sheet, cause hysteresis in electronic transport[23]. This bistable behaviour has opened up a new path to implement graphene-based electronic memory devices using electrochemical modification[24], graphene oxide[25] or ferroelectric materials[26]. On the other hand, a hysteretic change in the optical conductivity of graphene, induced by charge carrier retention or delayed response in reaching equilibrium, will provide potential photonic memory applications, similar to phase-change memory metamaterials[27]. Here, we present an electrically controllable light–matter interaction in a hybrid material/metamaterial system consisting of artificially constructed meta-atoms and truly two-dimensional carbon atoms. The extraordinary electrical and optical properties of graphene, when enhanced by the strong resonance of meta-atoms, lead to light–matter interaction of an unprecedented degree such that persistent switching and linear modulation of terahertz wave transmission are realized in the extreme subwavelength scale ($<\lambda/1{,}000{,}000$).

The structure of a fully integrated, gate-controlled, active terahertz graphene metamaterial is depicted schematically in Fig. 1a. Functionally, an array of meta-atoms, an atomically thin graphene layer and an array of metallic wire gate electrodes are configured together into an ultra-compact, thin and flexibly polymeric substrate (for details on the fabrication of the device, see Methods and Supplementary Fig. S1). In order not to complicate the underlying physics of the planar metamaterial layer without loss of generality, meta-atoms composed of a hexagonal metallic frame or asymmetric double split rings (aDSRs) exhibiting Fano-like resonance are periodically arranged (Fig. 1b). Large-area graphene grown by a chemical vapour deposition (CVD) process[28] is transferred onto the meta-atom layer (see Supplementary Section SI for the characterization of single-layer graphene (SLG) and multilayer graphene (MLG)). For gate-controllable doping of the graphene, three electrodes are incorporated into the metamaterial

[1]Department of Mechanical Engineering, Korea Advanced Institute of Science and Technology (KAIST), Daejeon 305-751, Republic of Korea, [2]Creative Research Center for Graphene Electronics, Electronics and Telecommunications Research Institute (ETRI), Daejeon 305-700, Republic of Korea, [3]Nanoscale Science and Engineering Center, 3112 Etcheverry Hall, University of California, Berkeley, California 94720, USA, [4]Department of Electrical Engineering, Korea Advanced Institute of Science and Technology (KAIST), Daejeon 305-751, Republic of Korea, [5]Materials Science Division, Lawrence Berkeley National Laboratory, 1 Cyclotron Road, Berkeley, California 94720, USA. †These authors contributed equally to this work.
*e-mail: bmin@kaist.ac.kr.

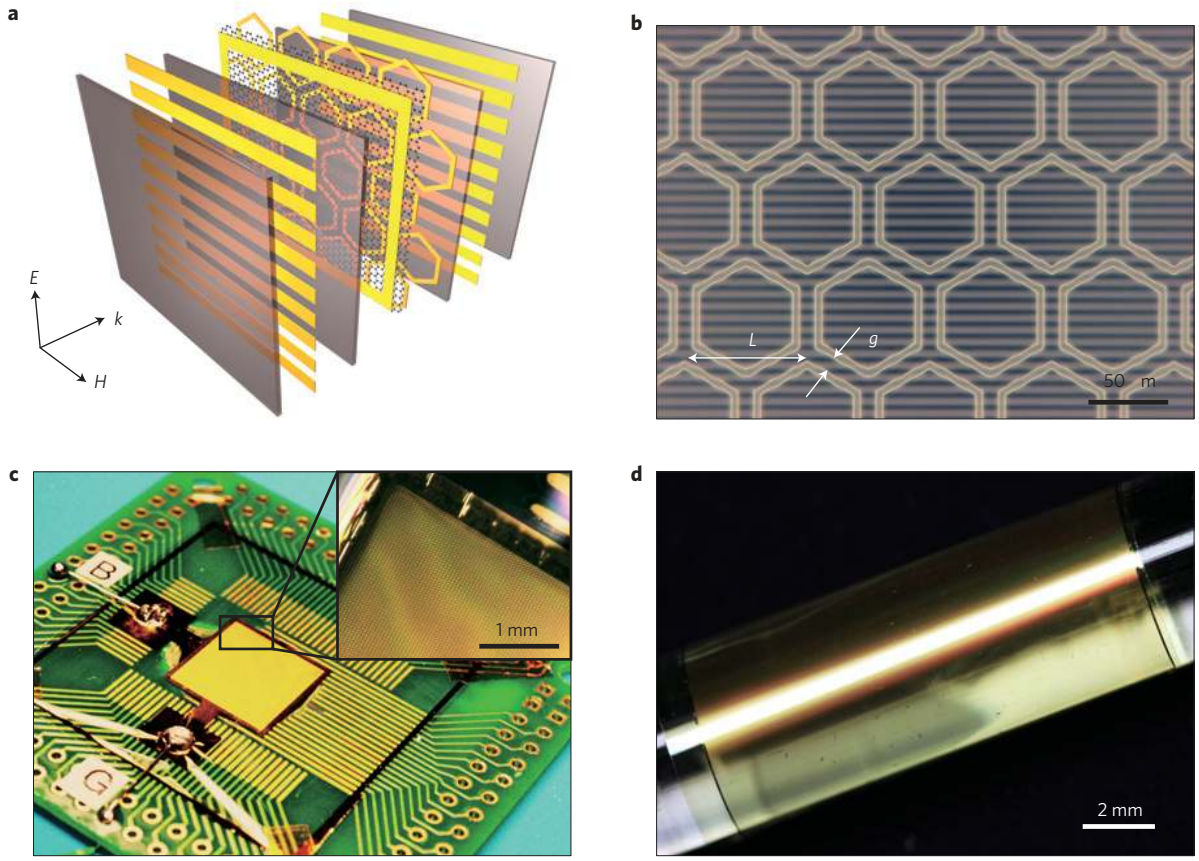

Figure 1 | Schematic view and device images of gate-controlled active graphene metamaterials. a, Schematic rendering of a gate-controlled active graphene metamaterial composed of a SLG deposited on a layer of hexagonal metallic meta-atoms (a unit cell of $L = 60\,\mu m$ and $g = 5\,\mu m$) and top/bottom EOT electrodes (periodicity $= 6\,\mu m$, metal width $= 4\,\mu m$) embedded in a dielectric material of $4.22\,\mu m$ thickness. Metallic patterns and dielectric materials are represented by yellow and grey, respectively. The polarization of the incident terahertz wave is perpendicular to the line electrode, as indicated by the arrows. **b**, Optical micrograph of the fabricated gate-controlled active graphene metamaterial without the top electrode. **c**, Fully integrated gate-controlled active graphene metamaterial attached to a drilled PCB for THz-TDS measurement (B, connected to bottom EOT electrode; G, connected to graphene layer). Inset: magnified view of the gate-controlled active graphene metamaterial. **d**, Optical image of the fabricated large-area metamaterial wound around a glass rod, showing its high degree of flexibility.

device, two of which are attached on both the top and bottom polyimide spacers surrounding the graphene/meta-atom layer (Fig. 1a), and the other electrode is directly connected to the graphene layer (ground). The top and bottom electrodes are carefully designed to apply a static electric field near the periphery of the graphene layer, while allowing incident terahertz radiation to be transmitted without being perturbed by these electrodes. For this purpose, these electrodes are constructed with a thin metallic wire array, where the gap between adjacent wires is in the deep-subwavelength scale ($\sim\lambda/150$) to fully use the extraordinary optical transmission[29] (EOT) of terahertz waves (see Supplementary Section SII for details of the EOT electrodes). By applying the gate voltage to one of the EOT electrodes, the Fermi level of the graphene, and hence the carrier density, can be dynamically controlled with a corresponding change of conductivity. This modified optical conductivity is translated into the variation of the complex permittivity of the atomically thin graphene layer, which in turn results in changes to the transmitted terahertz wave through the metamaterial. An optical micrograph of the fabricated graphene metamaterial attached to a printed circuit board (PCB) is shown in Fig. 1c. As shown in Fig. 1d, the fabricated active graphene metamaterial is large-area ($15 \times 15\,mm^2$), fully flexible and free-standing without the thick base substrate that is generally required for semiconductor-based terahertz modulators.

Terahertz time-domain spectroscopy (THz-TDS) was employed to measure amplitude and phase changes in terahertz waves transmitted through the gate-controlled active graphene metamaterial with variations in the applied gate voltage V_g. The experimentally measured transmission spectra of the SLG metamaterial (with hexagonal meta-atoms) clearly show the gate-voltage-dependent resonant features (Fig. 2a): the resonance frequency (f_0) is redshifted with increasing $|\Delta V|$, where $|\Delta V| = |V_{CNP} - V_g|$ and V_{CNP} is the charge neutral gate voltage. This redshift is mainly due to the increase in the real part of the complex conductivity of graphene; the width of the resonance is broadened with increasing $|\Delta V|$, which is caused by increased Joule losses in the metallic graphene layer; the on-resonance transmission, $T(f_0)$, increases for the SLG metamaterial as a result of the weaker resonant strength of meta-atoms with increasing real part of the complex conductivity of the graphene layer (Fig. 2g); and the off-resonance transmission is suppressed with increasing $|\Delta V|$ owing to the gate-induced broadband electro-absorption in the graphene layer. The V_{CNP} of the device under test is estimated to be $\sim 350\,V$ from the measured trace of transmission minima (dashed line in Fig. 2a). To quantify the active tuning capability more clearly, relative changes in transmission with respect to the charge neutral point (CNP), $-\Delta T/T_{CNP}$ (where $\Delta T = T - T_{CNP}$), are plotted as a function of V_g, as shown in Fig. 2b. At the maximum $\Delta V = 850\,V$, the measured $-\Delta T/T_{CNP}$ reaches approximately

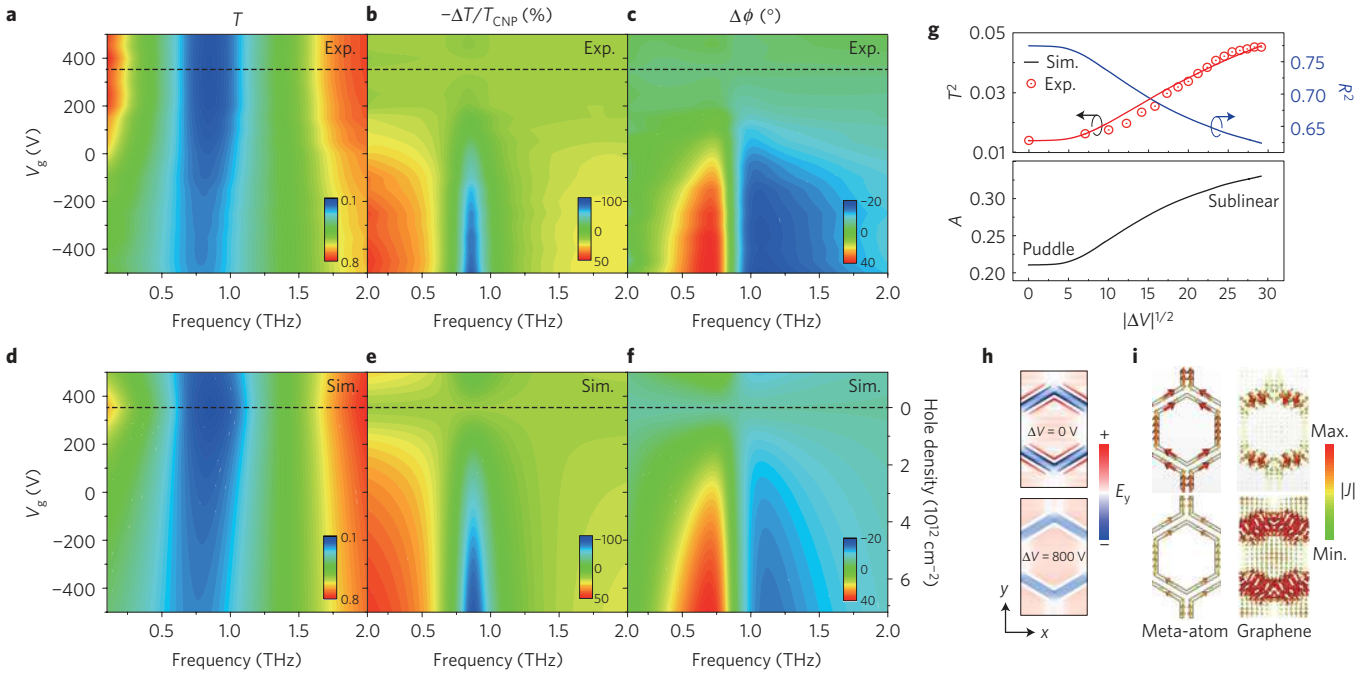

Figure 2 | Gate-controlled amplitude and phase changes of terahertz waves transmitted through the hexagonal graphene metamaterials. a–c, Measured spectra of transmission (T; **a**), relative change in transmission ($-\Delta T/T_{CNP}$; **b**), phase change ($\Delta\phi$; **c**) plotted as a function of gate voltage. **d–f**, Plots of simulated results with a SLG approximation, corresponding to **a–c**, respectively. Scattering time $\tau = 16$ fs and carrier density at the conductivity minimum $n_0 = 4 \times 10^{11}$ cm^{-2} are assumed for the simulations. **g**, Measured on-resonance intensity transmission (T^2), reflection (R^2) and absorption (A) plotted as a function of $|\Delta V|^{1/2}$ along with the simulated intensity transmission curve. Scatters and lines are for the experimental and simulated data, respectively. **h**, Saturated electric field (at 0.86 THz) within a unit cell for the graphene metamaterial with (lower panel) and without applying gate voltage (upper panel). **i**, Current density (at 0.86 THz) in the meta-atom (left panel) and the graphene layer (right panel) with increasing gate voltage.

-90% ($-\Delta T/T_{max} \simeq -47\%$) when the frequency approaches f_0 in the SLG metamaterial. In the case of a MLG metamaterial, the measured $-\Delta T/T_{CNP}$ exceeds -138% ($-\Delta T/T_{max} \simeq -58\%$) with a relatively small $\Delta V = 120$ V (see Supplementary Section SIII for the MLG metamaterials). It is noteworthy that this huge modulation is achieved solely by the inclusion of a graphene layer of infinitesimal thickness ($<\lambda/1{,}000{,}000$ for SLG) into the metamaterial of deep-subwavelength-scale thickness ($\sim\lambda/100$). The relative change in transmission per unit thickness was measured to be $-\Delta T/(T_{max}d) \simeq -14\%\,\mu m^{-1}$ (for the MLG metamaterial), which exceeds that of all previously reported 2DEG- and metamaterial-based terahertz modulators. Moreover, a large degree of broadband modulation at the off-resonance frequencies (0.1–0.6 and 1.2–2.5 THz) is possible because the real part of the complex conductivity of graphene shows negligible dispersion over the frequency ranges from 0 to 2.5 THz. Figure 2c shows the measured phase change $\Delta\phi$ in SLG metamaterials as a function of V_g. One of the most intriguing aspects made possible by incorporating a resonant element in an active medium is the ability to modulate the phase of transmitting terahertz waves to a considerable degree. The maximum value of $\Delta\phi$ in SLG metamaterials exceeds 32.2° at 0.65 THz ($\Delta\phi \simeq 65°$ for the MLG graphene metamaterial, see Supplementary Section SIII). This substantial gate-controlled phase modulation of terahertz waves can be further increased by reducing the gap between the hexagonal meta-atoms and/or by stacking multiple layers of deep-subwavelength-scale graphene metamaterial[13]. The modulation speed of the active graphene metamaterial exceeds at least 100 kHz (see Supplementary Section SIV).

For a quantitative comparison with experimentally observed phenomena, the transmission spectra of active graphene metamaterials were calculated by a finite element analysis. To model the atomically thin graphene layer in electromagnetic wave simulations, the complex conductivity of graphene estimated using Kubo's formula was converted to a dielectric constant for a very thin effective layer[7]. The conductivity of graphene ($\sigma_g = \sigma_{inter} + \sigma_{intra}$) at terahertz frequencies is dominated by the contribution from the intraband transition and can be cast approximately in a Drude-like form (see Supplementary Section SIV for simulation method). The applied gate voltage leads to a carrier density change and consequently shifts the Fermi level (E_F) according to the following formula (for SLG): $|E_F| = \hbar v_F(\pi N)^{1/2}$, where $v_F \approx 1 \times 10^6$ m s^{-1} is the Fermi velocity, N is the total carrier density given by $N = (n_0^2 + \alpha^2|\Delta V|^2)^{1/2}$, n_0 is the residual carrier concentration induced by density fluctuation due to charged impurities near the Dirac point, and $\alpha \approx 8.54 \times 10^9$ cm^{-2} V^{-1} is the EOT gate capacitance in the electron charge, respectively. Inserting these values into Kubo's formula, the transmission (Fig. 2d), the relative change in transmission (Fig. 2e) and phase change (Fig. 2f) were calculated as a function of gate-voltage changes. Most of the gate-voltage-dependent resonant features were excellently reproduced in the simulations with the following fitting parameters: scattering time $\tau = 16$ fs and carrier density at the conductivity minimum $n_0 = 4 \times 10^{11}$ cm^{-2}. The fitted scattering time and the carrier density at the conductivity minimum are comparable to those previously reported for thermally grown graphene[30,31]. It is worth noting that the nonlinear change in transmission can hardly be fitted with the bilayer approximation[32], which provides further evidence on the embedded SLG (SLG characterization using Raman spectroscopy[33] is given in the Supplementary Section SI). For a better understanding of the gate-voltage-dependent light–matter interaction in the graphene metamaterials, the on-resonance intensity transmission (T^2), reflection (R^2) and absorption are plotted as a function of $|\Delta V|^{1/2}$ in Fig. 2g. As clearly seen from the plot in Fig. 2g, three distinct scaling regimes were clearly identified in the plots with respect to $|\Delta V|^{1/2}$; a puddle regime where the Fermi level changes

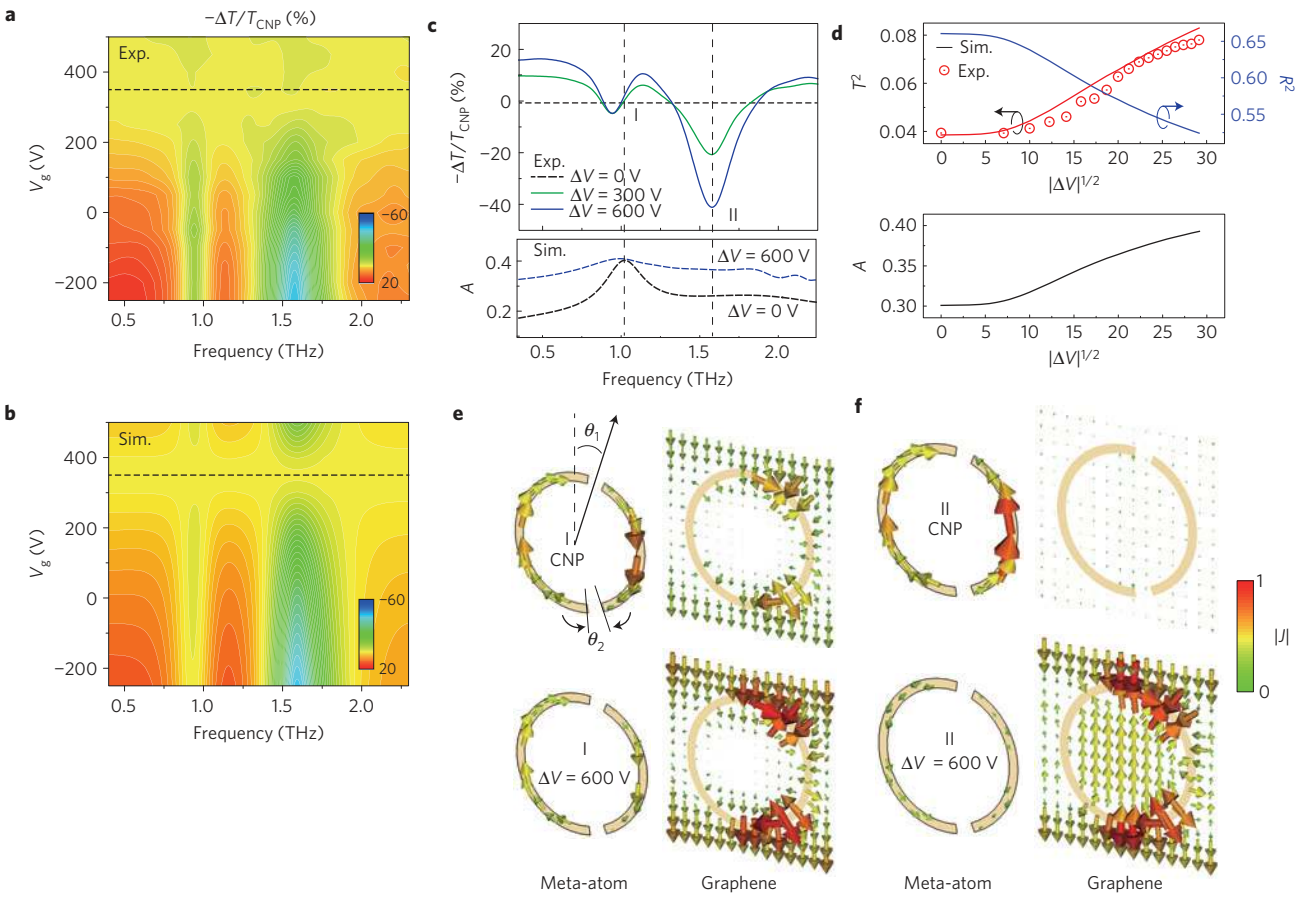

Figure 3 | Gate-controlled amplitude change of terahertz waves transmitted through the aDSR graphene metamaterials. a, Measured relative change in transmission of the aDSR graphene metamaterials plotted as a function of gate voltage. **b**, Simulated results obtained with the SLG approximation show good agreement with experimental observation. **c**, Two distinct resonances are marked I (trapped mode) and II (dipole mode) with different tuning behaviours. As the gate voltage increased, transmission at the dipole mode resonance significantly increased; however, the trapped mode transmission showed little change, where the origin is from a small change in the absorption for the trapped mode (lower panel). **d**, Measured on-resonance intensity transmission, reflection and absorption for the dipole mode plotted as a function of $|\Delta V|^{1/2}$ along with the simulated intensity transmission curve. **e**, Gate-dependent current density for the trapped mode is shown with the arrows in a unit cell of a aDSR meta-atom (left panel) and a graphene layer (right panel). **f**, Corresponding current density for the dipole mode.

weakly with $|\Delta V|^{1/2}$ owing to the charged impurities[34], a linear regime where the Fermi level scales linearly with $|\Delta V|^{1/2}$, and a sublinear regime where the short-range scattering of charge carriers dominates (the effect of short-range scattering was not taken into account in the simulation). Detailed dynamics of charge carrier transport can be clearly visualized with the numerical simulation. At the CNP, the conductivity of the graphene layer is still small enough so as not to perturb the inductor–capacitor (LC) resonance of hexagonal meta-atoms. With increasing $|\Delta V|$, the graphene becomes more conductive such that fewer charge carriers accumulate at the edge of the meta-atoms as charge carriers can leak into adjacent meta-atoms through conductive graphene channels, as shown in the field simulation depicted in Fig. 2h,i.

To investigate gate-controlled behaviours in an artificial multi-resonance system hybridized with SLG, aDSRs (ref. 35) are used as a unit cell of meta-atoms. Figure 3 shows the gate-dependent transmission for aDSR graphene metamaterial. With broken symmetry in aDSR meta-atoms (asymmetric factors of $\theta_1 = 15°$ and $\theta_2 = 10°$ are defined in Fig. 3e), a sharp Fano-like resonance (trapped mode, marked as I in Fig. 3c) is observed in the low-frequency side of the fundamental electric dipole mode resonance (marked as II in Fig. 3c). The simulated current densities for these two distinct modes in aDSRs are depicted by the arrows in the left panel inside Fig. 3e,f. Compared with the electric dipole mode (in-phase current oscillation), the trapped mode resonance (out-of-phase current oscillation) exhibits a higher quality factor due to weak free-space coupling and low radiation losses. At the trapped mode resonance, the absorption of the metamaterial reaches a maximum value of 40%, the main contribution arising from substrate and metallic losses (the intrinsic terahertz absorption in the graphene layer is substantially lower at the CNP (ref. 10)). As we increased the gate voltages, absorption increased substantially, except in the vicinity of the Fano-like resonance, by carrier-induced electro-absorption in the SLG (lower panel of Fig. 3c). Hence, the gate-dependent transmission changes showed different behaviours for these two modes. The on-resonance transmission of the trapped mode showed little change ($-\Delta T/T_{\mathrm{CNP}} < 5\%$) with gate voltages, whereas for the electric dipole mode, the changes are substantial, amounting to about -40% ($-\Delta T/T_{\max} \simeq -30\%$). Similar to the case for the hexagonal meta-atom structure, the on-resonance intensity transmission, reflection and absorption scale nonlinearly for the dipole mode as shown in Fig. 3d. Such broadband tunable absorption means that the graphene metamaterial could be used as a platform to attain a perfect absorber by patterning and/or stacking graphene layers.

In addition to promising amplitude and phase modulation predictable on the basis of the carrier dynamics of ideal graphene, active graphene metamaterial exhibits a considerable amount

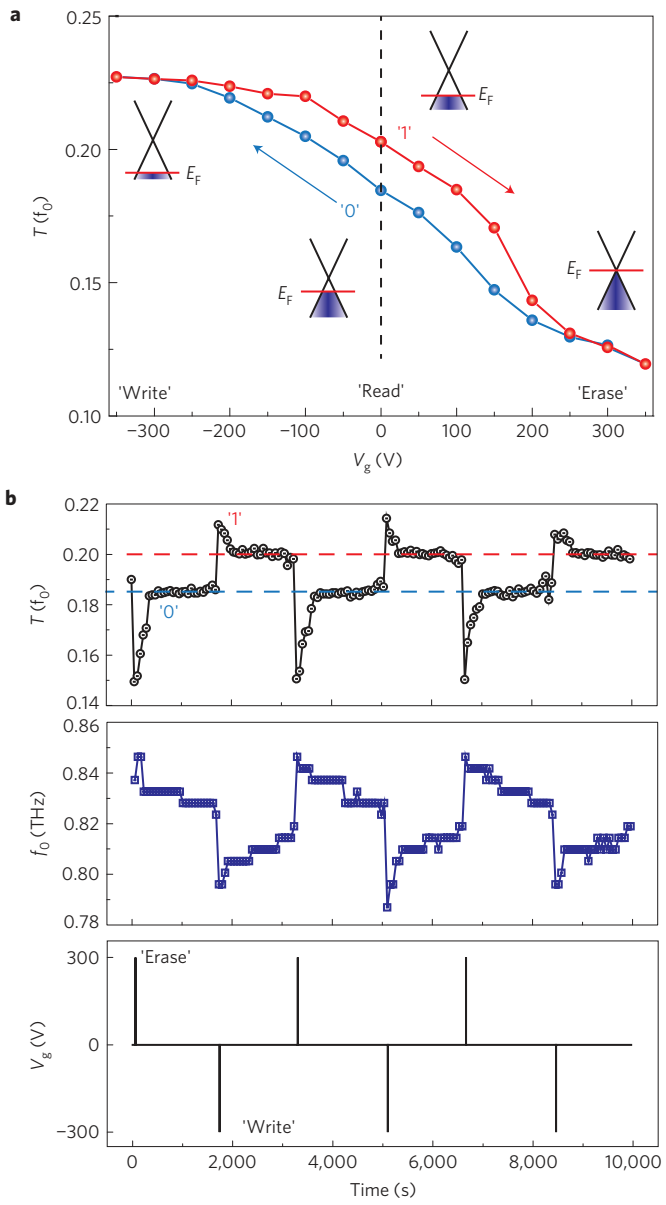

Figure 4 | Electrically controlled photonic memory operation with the gate-controlled active graphene metamaterials. a, Hysteresis behaviour of on-resonance transmission for a cyclic change of the gate voltage (with a sweeping rate of 50 V min^{-1}). In the insets, the Fermi level of the graphene is schematically illustrated for each of the operating points. **b**, Binary memory operation in the transmission (top panel), a measured time-trace of resonance frequency (middle panel), and gating pulse signal (pulse width = 1 s, lower panel). The observed memory retention time is estimated to be around 20 min.

of gate-controlled optical hysteresis. The controllable hysteretic behaviours in the realistic graphene on a substrate[23–26], when combined with the metamaterial, can alternatively be used as a route towards the development of an electrically controllable photonic memory. The photonic memory effect in our device can be mainly attributed to charge trapping phenomena at the grain boundaries or defect sites (non-idealities in a large-area CVD-grown graphene layer) as well as adsorption of H_2O molecules on the polyimide substrate (see Supplementary Section SIV for the effect of humidity on the memory operation). Figure 4a shows such hysteretic behaviour in the transmission at a fixed frequency for a cyclic change of the gate voltage (for active graphene metamaterial with hexagonal meta-atoms). For this measurement, the gate voltage was swept at a rate of 50 V min^{-1}. Figure 4b shows a flip–flop operation in transmission (top panel) and a time-trace of measured resonance frequency (middle panel). Here, the write (set) and erase (reset) inputs were implemented by applying a short pulse signal of the gate voltage (pulse width = 1 s, lower panel). The peak gate voltage of pulses was set to −300 V (write) and 300 V (erase), respectively. The state of the transmission and/or resonance frequency of the SLG metamaterial was read at zero gate voltage ($V_g = 0$ V, dashed line in Fig. 4a). It is worth noting that the measured retention time of the active graphene metamaterial was proportional to both the magnitude and the pulse width of the applied gate voltage. With the given gate voltage pulses (±300 V for 1 s), the retention time is estimated to be around 20 min, which is comparable to the value of CVD-grown SLG ferroelectric memory[26] (Fig. 4b). For longer memory retention times, oxidative graphene would be superior to an intrinsic graphene layer owing to oxygen-related, stable memristive phenomena[23,24].

The exotic electrical and optical properties of graphene, when enhanced by the strong resonance of meta-atoms, lead to a very strong light–matter interaction in a manner that allows persistent switching and linear modulation of low-energy photons in the extreme-subwavelength scale ($\sim\lambda/1{,}000{,}000$). Surprisingly, low-energy photons were fully controlled while being transmitted through gate-controlled, one-atom-thick, SLG integrated with strongly coupled meta-atoms. The controllable light–matter interaction, as well as the memory effect in the active graphene metamaterials, presents immense potential for a myriad of important applications, particularly in active control of terahertz waves in the extreme-subwavelength scale, such as fast terahertz modulators, tunable transformation-optics devices, electrically controllable photonic memory and reconfigurable terahertz devices.

Methods

Fabrication processes for the gate-controlled active graphene metamaterial. All metallic parts of the graphene metamaterial were made of 100-nm-thick gold with a 10-nm-thick chromium adhesion layer. Graphene was grown by CVD to cover the entire area of the metamaterial (15 × 15 mm^2). A bare silicon wafer was used as a sacrificial substrate. To construct the active graphene metamaterial on the sacrificial substrate, a polyimide solution (PI-2610, HD MicroSystems) was spin-coated and fully cured using a two-step baking process, resulting in a final polyimide thickness of 1 μm. To define the bottom EOT electrode on the prepared polyimide layer, ultraviolet photolithography and electron-beam evaporation were followed by a metal lift-off technique. Repeating the same polyimide stacking processes as employed for the first layer, the metallic meta-atoms are then insulated from the bottom electrode. The metallic meta-atoms were patterned using the same processes as for the bottom electrode. Then, the graphene (SLG on Cu foil, MLG on Ni/SiO_2/Si substrate) was transferred and conformally attached to the array of meta-atoms. After the graphene layer had been transferred onto the meta-atoms, a ground electrode was defined on the graphene layer using a shadow mask. For the symmetry of graphene metamaterials in the direction of the terahertz wave propagation, a polyimide layer and a top EOT electrode (optional) were stacked. After opening the electrical contact using O_2 plasma etching, the free-standing and flexible active graphene metamaterials were peeled off the silicon substrate. Finally, the active graphene metamaterials were soldered to a drilled PCB substrate.

THz-TDS system. For the generation of broadband terahertz waves, a Ti:sapphire femtosecond oscillator (Mai-Tai, Spectra-physics) with a pulse repetition rate of 80 MHz was used. The pulse width is approximately 100 fs. The central wavelength and average power of the oscillator were set to 800 nm and 1 W, respectively. The pulsed laser beam was focused onto a biased, low-temperature-grown GaAs terahertz emitter (Tera-SED, Gigaoptics). The modulation frequency and the duty cycle of the rectangular bias voltage (−10–10 V) were 1 kHz and 50%, respectively (except for the measurement of modulation speed of the graphene metamaterial, in which case the modulation frequency was swept from 1 to 100 kHz). The emitted terahertz wave was then guided and focused onto the samples with a 2-mm-diameter spot by using off-axis parabolic mirrors. The maximum field amplitude at the focal spot was estimated to be ~1 kV cm^{-1}. The propagating terahertz radiation was detected electro-optically using a 1-mm-thick and 110-oriented ZnTe crystal. The THz-TDS system has a usable bandwidth of 0.1–2.6 THz and a signal-to-noise ratio of over 10,000:1.

Received 13 March 2012; accepted 24 August 2012; published online 30 September 2012

References

1. Geim, A. K. & Novoselov, K. S. The rise of graphene. *Nature Mater.* **6,** 183–191 (2007).
2. Wang, F. *et al.* Gate-variable optical transitions in graphene. *Science* **320,** 206–209 (2008).
3. Bonaccorso, F., Sun, Z., Hasan, T. & Ferrari, A. C. Graphene photonics and optoelectronics. *Nature Photon.* **4,** 611–622 (2010).
4. Ju, L. *et al.* Graphene plasmonics for tunable terahertz metamaterials. *Nature Nanotech.* **6,** 630–634 (2011).
5. Koppens, F. H. L., Chang, D. E. & De Abajo, F. J. G. Graphene plasmonics: A platform for strong light–matter interactions. *Nano Lett.* **11,** 3370–3377 (2011).
6. Liu, M. *et al.* A graphene-based broadband optical modulator. *Nature* **474,** 64–67 (2011).
7. Vakil, A. & Engheta, N. Transformation optics using graphene. *Science* **332,** 1291–1294 (2011).
8. Echtermeyer, T. J. *et al.* Strong plasmonic enhancement of photovoltage in graphene. *Nature Commun.* **2,** 458 (2011).
9. Papasimakis, N. *et al.* Graphene in a photonic metamaterial. *Opt. Express* **18,** 8353–8359 (2010).
10. Maeng, I. *et al.* Gate-controlled nonlinear conductivity of Dirac fermion in graphene field-effect transistors measured by terahertz time-domain spectroscopy. *Nano Lett.* **12,** 551–555 (2012).
11. Pendry, J. B., Holden, A. J., Robbins, D. J. & Stewart, W. J. Magnetism from conductors and enhanced nonlinear phenomena. *IEEE Trans. Microw. Theory Tech.* **47,** 2075–2084 (1999).
12. Smith, D. R., Padilla, W. J., Vier, D. C., Nemat-Nasser, S. C. & Schultz, S. Composite medium with simultaneously negative permeability and permittivity. *Phys. Rev. Lett.* **84,** 4184–4187 (2000).
13. Choi, M. *et al.* A terahertz metamaterial with unnaturally high refractive index. *Nature* **470,** 369–373 (2011).
14. Ferguson, B. & Zhang, X-C. Materials for terahertz science and technology. *Nature Mater.* **1,** 26–33 (2002).
15. Hu, T., Padilla, W. J., Xin, Z. & Averitt, R. D. Recent progress in electromagnetic metamaterial devices for terahertz applications. *IEEE J. Sel. Top. Quan. Electron.* **17,** 92–101 (2011).
16. Kleine-Ostmann, T., Dawson, P., Pierz, K., Hein, G. & Koch, M. Room-temperature operation of an electrically driven terahertz modulator. *Appl. Phys. Lett.* **84,** 3555–3557 (2004).
17. Sensale-Rodriguez, B. *et al.* Unique prospects for graphene-based terahertz modulators. *Appl. Phys. Lett.* **99,** 113104 (2011).
18. Chen, H. T. *et al.* Active terahertz metamaterial devices. *Nature* **444,** 597–600 (2006).
19. Chen, H-T. *et al.* A metamaterial solid-state terahertz phase modulator. *Nature Photon.* **3,** 148–151 (2009).
20. Shrekenhamer, D. *et al.* High speed terahertz modulation from metamaterials with embedded high electron mobility transistors. *Opt. Express* **19,** 9968–9975 (2011).
21. Das, A. *et al.* Monitoring dopants by Raman scattering in an electrochemically top-gated graphene transistor. *Nature Nanotech.* **3,** 210–215 (2008).
22. Efetov, D. K. & Kim, P. Controlling electron-phonon interactions in graphene at ultrahigh carrier densities. *Phys. Rev. Lett.* **105,** 256805 (2010).
23. Wang, H. M., Wu, Y. H., Cong, C. X., Shang, J. Z. & Yu, T. Hysteresis of electronic transport in graphene transistors. *ACS Nano* **4,** 7221–7228 (2010).
24. Echtermeyer, T. J. *et al.* Nonvolatile switching in graphene field-effect devices. *IEEE Electron Device Lett.* **29,** 952–954 (2008).
25. Jeong, H. Y. *et al.* Graphene oxide thin films for flexible nonvolatile memory applications. *Nano Lett.* **10,** 4381–4386 (2010).
26. Song, E. B. *et al.* Robust bi-stable memory operation in single-layer graphene ferroelectric memory. *Appl. Phys. Lett.* **99,** 042109 (2011).
27. Driscoll, T. *et al.* Memory metamaterials. *Science* **325,** 1518–1521 (2009).
28. Kim, K. S. *et al.* Large-scale pattern growth of graphene films for stretchable transparent electrodes. *Nature* **457,** 706–710 (2009).
29. Martín-Moreno, L. *et al.* Theory of extraordinary optical transmission through subwavelength hole arrays. *Phys. Rev. Lett.* **86,** 1114–1117 (2001).
30. Dawlaty, J. M. *et al.* Measurement of the optical absorption spectra of epitaxial graphene from terahertz to visible. *Appl. Phys. Lett.* **93,** 131905 (2008).
31. Li, X. *et al.* Large-area synthesis of high-quality and uniform graphene films on copper foils. *Science* **324,** 1312–1314 (2009).
32. Yu, Y-J. *et al.* Tuning the graphene work function by electric field effect. *Nano Lett.* **9,** 3430–3434 (2009).
33. Ferrari, A. C. *et al.* Raman spectrum of graphene and graphene layers. *Phys. Rev. Lett.* **97,** 187401 (2006).
34. Adam, S., Hwang, E. H., Galitski, V. M. & Das Sarma, S. A self-consistent theory for graphene transport. *Proc. Natl Acad. Sci. USA* **104,** 18392–18397 (2007).
35. Fedotov, V. A., Rose, M., Prosvirnin, S. L., Papasimakis, N. & Zheludev, N. I. Sharp trapped-mode resonances in planar metamaterials with a broken structural symmetry. *Phys. Rev. Lett.* **99,** 147401 (2007).

Acknowledgements

We thank B. H. Hong for the discussion on the application of graphene, Y-J. Yu for the discussion on carrier transport in graphene, J. H. Han for the characterization of graphene, and H. Choi for proofreading the manuscript. This work was supported by the National Research Foundation of Korea (NRF) grant funded by the Korea government (MEST) (No. 2008-0062235, 2009-0069459, 2010-0012058, 2011-0020186 and 2011-0028151). S.S.L. acknowledges the support by the NRF of Korea grant funded by the MEST (No.2010-0027050). S-Y.C. acknowledges the GFR Program (2011-0031640) sponsored by the MEST. C-G.C. acknowledges the Nano R&D Program (2011-0019169) through the NRF of Korea funded by the MEST and the Creative Research Program of the ETRI (11YF1110). X.Z. acknowledges the support from the US Department of Energy under contract no. DE-AC02-05CH11231 through Materials Sciences Division of Lawrence Berkeley National Laboratory (LBNL).

Author contributions

S.H.L., M.C., T-T.K. and B.M. conceived the original idea. S.H.L. and M.C. fabricated the samples. T-T.K., S.H.L. and M.C. performed the experiments. S.H.L., M.C., S.L., M.L., H.K.C., C-G.C., S-Y.C. and B.M. characterized the graphene. S.H.L., M.C., T-T.K., S.L., M.L., X.Y., S.S.L., S-Y.C., X.Z. and B.M. analysed the data and discussed the results. S.H.L., M.C., T-T.K., S.L., M.L., X.Z. and B.M. wrote the paper, and all authors provided feedback.

Additional information

Supplementary information is available in the online version of the paper. Reprints and permissions information is available online at www.nature.com/reprints. Correspondence and requests for materials should be addressed to B.M.

Competing financial interests

The authors declare no competing financial interests.